An Analytical Method for Three-Dimensional Nonlinear Responses of Prestressed Concrete Nuclear Reactor Vessels

Katsuyoshi Imoto

プレストレスト・コンクリート製圧力容器の三次元弾塑性解析法

井 元 勝 慶

概　　要

プレストレスト・コンクリート製原子炉圧力容器 (PCRV) などの三次元厚肉コンクリート構造物が単調載荷を受ける際の材料非線形応答を求める数値解析方法を提案し，この方法による解をPCRVテストモデルの実験結果と比較検討した結果について述べる。

三軸応力状態のコンクリートの破壊面として二重破壊条件の概念を採用することによって，圧縮側と引張側の応力状態に対して，それぞれ独立した破壊面を設定した。この破壊面は，(1)引張側で中間主応力の影響を考慮した関数によって近似され，圧縮側では一般化された Drucker-Prager の条件式によって表わされている。(2)圧縮側での非線形挙動は弾塑性理論に基づいた応力—ひずみ関係でモデル化されている。

この非線形応力—ひずみ関係では，相当塑性ひずみとそのときの応力状態に依存する有効ひずみ硬化係数を導入することによって，非線形域における応力—ひずみ関係が各種応力経路によって異なるという実験的事実を近似できるようモデル化されている。これらの手法と三次元有限要素法を用いて，鉄筋コンクリート構造物解析プログラムを開発した。この方法の妥当性を検討するために，二次元コンクリートと軸対称および三次元形状をしたPCRVテストモデルの三例を解析した。その結果，この方法による解析は，十分にPCRVの非線形挙動を予測できることが確認された。なお，この解法は一般の三次元鉄筋コンクリートの材料非線形解析法として有効かつ実用的なものと思われる。

Abstract

This report describes the results of an investigation to develop an analytical method for the nonlinear behaviors and strengths of three-dimensional reinforced concrete structures such as prestressed concrete nuclear reactor vessels (PCRV) under monotonically increasing internal pressure. The mathematical model for concrete has the following features. A model of a "dual failure criterion" was adopted to simulate the failure surface for all stages of stress. That is, (1) in compression, failure is controlled by a generalized Drucker-Prager criterion proposed, satisfying convexity and continuity conditions, and (2) in tension-tension and tension-compression, the cracking criterion reflects the effect of the intermediate principal stress by use of the tension cut-off criterion. A method of modifying the effect of microcracking in compression on nonlinear response was incorporated in the yield criterion by use of an exponential approximation function in terms of current stress state and equivalent plastic strain. A nonlinear finite element computer program was established in a suitable form for general use incorporating the mathematical model proposed. Three numerical examples, such as two-, three-dimensional, and axisymmetrical problems, were analyzed to investigate the feasibility of the procedure developed. Good agreement between experimental and analytical results was obtained. As a result, it was found possible to predict the nonlinear responses of massive reinforced concrete structures like PCRV.

1. Introduction

With the recent remarkable advances in finite element techniques together with the progress of high speed digital computers and many though insufficient experimental investigations

on the material phenomena of concrete under multiaxial stress state, three-dimensional nonlinear analysis procedures of the PCRV have been proposed by assuming mathematical models for concrete on the basis of the available limited experimental data and comparing the calculated results with the PCRV test results. Nevertheless, the applicability of most analytical methods for general use are still questionable by the reason that few of these have been applied to many PCRV models because of economics. Moreover, there is no generally accepted constitutive law to characterize the nonlinear response of concrete under multiaxial stress state in all stages of loading.

The object of this investigation is to provide an analytical procedure which can predict the nonlinear response of PCRV to accidental overpressurization over a short period of time. The analytical method developed is three-dimensional and uses a material model, related to the elastic-plastic theory, proposed here for the nonlinear response of concrete under multiaxial stress state.

2. Constitutive Modeling for Plain Concrete under Multiaxial Stress State

A few experimental investigations on the strength and deformation behavior of concrete under multiaxial stress state have been carried out (1, 2, 3, 4). There are still many questions unanswered regarding the accuracy of these results. However, from the limited data, the shape of failure surface has been considered to be as shown in Fig. 1 in the deviatoric, hydrostatic and rendulic sections. Basically the failure surface is a conical surface with curved meridians and monlinear cross sections in which the shape is trigonal in tension while a cylindrical shape is approached in the limit in compression (2, 3).

2.1. Failure Surface

Various forms of expressions for the failure surface are currently used for the non-linear analysis of reinforced concrete structures (5, 6). There are in general two existing ways for the description of failure surface; a model which simulates the surface by a single function, and the other which is a model with two-independent functions dividing the surface into two parts (tension and compression zones). The latter, the so-called "dual failure criterion", is considered to be more reasonable than the former because of capability for the description of the surface by simple functions. Here a model based on the dual failure criterion will be developed to make the description simple and realistic.

Because of the triple symmetry at the principal stress axes as shown in Fig. 1. b, only a sixth of the surface has to be considered. Hence, it is specified that the principal stress components are ordered such that $\sigma_1 \geq \sigma_2 \geq \sigma_3$ and tensile stress is taken as positive. It can, in general, be assumed that the failure surface passes through five points (A, B, C, D, E) as shown in Fig. 2 in the hydrostatic plane (5). In this plane the full range of the surface may be divided into two zones; (I) compression zone above line $\overline{AB}$ and (II) tension-tension and tension-compression zones below line $\overline{AB}$.

2.1.1. Compression-Compression Zone (I) Equation (1), named a generalized Drucker-Prager failure criterion, is proposed as an approximate description of the surface in compression zone.

$$F_c = \alpha J_1 + \frac{\sqrt{J_2}}{g(\theta)} - K(\theta, \bar{\varepsilon}_p) \equiv 0 \tag{1}$$

where $\alpha = \dfrac{1}{\sqrt{3}\,(2\eta_b - 1)}(\eta_b/\beta - 1)$

β = material constant of ratio of radii at $\theta = 0°$ and $60°$ in the deviatoric section, $0.5 \leq \beta \leq 1.0$.

η_b = material constant of ratio of biaxial compressive strength, f_b, to uniaxial compressive strength f_c', i.e. $\eta_b = f_b/f_c'$

θ=Lode angle (6, 7) $=\frac{1}{3}\sin^{-1}\left(-\frac{3\sqrt{3}}{2}\frac{J_3}{\sqrt{J_2{}^3}}\right)+30°$, $0°\leq\theta\leq60°$

J_1, J_2, J_3=first, second and third stress invariants, respectively.

$J_1=\sigma_1+\sigma_2+\sigma_3$, $J_2=\frac{1}{2}S_{ij}S_{ij}$, $J_3=\frac{1}{3}S_{ij}S_{jk}S_{ki}$

S_{ij}=stress deviator tensor

$g(\theta)$=a hyperbolic interpolation function assumed in the deviatoric section, satisfying the continuity and boundary conditions, written as

$$g(\theta)=\beta\frac{2(1-\beta^2)\cos\theta-(2-\beta)[2(\beta^2-1)(1+\cos2\theta)+5-4\beta]^{1/2}}{2(1-\beta^2)(1+\cos2\theta)-(2-\beta)^2} \tag{2}$$

$K(\theta, \bar{\varepsilon}_p)$=equivalent stress depends on the current state of stress and plastic strain.

The surface described by Eq. 1 projects as a straight line along the meridian and as a noncircular shape on the deviatoric section. Note that if $\beta=1.0$, Eq.1 degenerates to the well-known Drucker-Prager yield criterion, and if $\beta=\eta_b=1.0$, Eq. 1 degenerates to the Von Mises yield criterion widely used for metal. The value of β, however, should be determined so that the function of Eq. 1 may simulate the variation of experimental data from compressive branch ($\theta=0°$) to tensile branch ($\theta=60°$) obtained by hydrostatic tests of plain concrete. According to the recent studies (2, 3, 4), the value of β is in the range between 0.7 and 0.8. Choice of the value also depends on whether it is failure in tension or compression range that should be simulated more closely. A value of $\beta=0.75$ gives a reasonable approximation in full range. Comparisons of the failure surface given in Eq. 1 with value of $\beta=0.75$ and the available experimental results are shown in Fig. 3, 4.

2.1.2. Tension-Tension and Tension-Compression Zones (II) Because the tensile strength, f_t', is about an order of magnitude less than f_c' and its failure is brittle, the nonlinear response of concrete structures are attributable primary to the tensile failure (cracking). The maximum principal stress (or strain) theory and Mohr-Coulomb theory have been frequently used to describe the failure. Current research on the tensile failure surface is moving toward the development of that including the effect of intermediate principal stress (5). Here, a tensile failure model taking account of this effect is proposed, which consists of two surfaces, one for tension-tension and the other for tension-compression zones with triangular shape in the deviatoric section. The model is defined by means of the octahedral shear and normal stresses and θ as

$$F_{ti}=\tau_{oct}-\frac{\sqrt{3}}{2}\frac{\tau_{Ai}\tau_{Bi}}{[\tau_{Ai}\sin\theta+\tau_{Bi}\sin(60-\theta)]}\equiv0 \quad (i=1,2) \tag{3}$$

where the terms of τ_{Ai}, τ_{Bi} are the extreme fixed octahedral shear stresses, corresponding to the meridians at $\theta=0°$ (line ACE) and $\theta=60°$ (line B'DE), respectively (Fig. 2). These can be written in terms of the current σ_m

$$\tau_{Ai}=A_{1i}\sigma_m+A_{2i}, \quad \tau_{Bi}=B_{1i}\sigma_m+B_{2i}, \quad (i=1,2) \tag{4}$$

Subscript i denotes that the function in case of $i=1$ indicates the surface for tension-compression zone where it passes through four points (A, C, B', D), and in case of $i=2$ indicates the surface for tension-tension zone where it passes through three points (C, E, D) as illustrated in Fig. 2. The constants can be easily determined from the figure.

For tension-compression zone ($i=1$)

$$A_{11}=\sqrt{2}(\beta_t-1)/(2\beta_t-1), \quad A_{21}=(\sqrt{2}+A_{11})/3$$
$$B_{11}=\sqrt{2}(\eta_b-\beta_t)/(3\chi-\beta_t), \quad B_{21}=\sqrt{2}\eta_b/3-\chi B_{11} \tag{5}$$

For tension-tension zone ($i=2$)

$$A_{12}=-\sqrt{2},\quad A_{22}=\sqrt{2}\beta_t,\quad B_{12}=-1/\sqrt{2},\quad B_{22}=\beta_t/\sqrt{2} \tag{6}$$

In the formation of Eq. 2, some consideration should be made for tension-compression zone. Point B' in Fig. 3 must be used in F_{t1} instead of point B, because adopting B makes the surface concave as a model in Ref. 5. By the study of Ref. 7, the coordinate of point B' in $\tau_{oct}-\sigma_m$ plane is approximately ($\chi=-0.7\sim-0.6$, $\sqrt{2}/3/\eta_b$). After some examination the value $\chi=-0.65$ gives better fit to experimental data. Note that the shape of F_{t2} is an equilateral triangle in the deviatoric section and this assures that the tensile failure surface never exceeds the tensile strength for any state of stress.

Consequently, the failure surface for full range can be determined by the function which reaches zero first among the three (F_c, F_{t1}, F_{t2}) in Eq. 1, 3. The characteristics of the failure surface proposed are figured by combination of the three independent functions in Fig. 5.

2.2. Incremental Stress-Strain Relationship in Compression

The model based on the elastic-plastic theory has been widely adopted for general use to describe the nonlinear behavior of reinforced concrete because of simplicity, systemized formulation of the constitutive law, and existence of reasonable results except in a certain limited stress region. The incremental stress-strain relationship developed is also based on the elastic-plastic theory with the basic assumptions that (1) the initial and subsequent yield surface are similar to the Generalized Drucker-Prager failure function given in Eq. 1, and (2) simple work hardening associated with the Reuss's flow rule, and can be written in the form

$$\{d\sigma\}=D^{ep}\{d\varepsilon\} \tag{7}$$

$$D^{ep}=D^e-D^e\left\{\frac{\partial F}{\partial\sigma}\right\}\left\{\frac{\partial F}{\partial\sigma}\right\}^T D^e\left[H'+\left\{\frac{\partial F}{\partial\sigma}\right\}^T D^e\left\{\frac{\partial F}{\partial\sigma}\right\}\right]^{-1} \tag{8}$$

where D^e is the elastic strain to stress transfer matrix, the term H' is effective strain hardening coefficient. The rate $\{\partial F/\partial\sigma\}$ is the gradient vector of stress components and can be conveniently expressed as

$$\left\{\frac{\partial F}{\partial\sigma}\right\}=\frac{\partial F}{\partial J_1}\left\{\frac{\partial J_1}{\partial\sigma}\right\}+\frac{\partial F}{\partial J_2}\left\{\frac{\partial J_2}{\partial\sigma}\right\}+\frac{\partial F}{\partial J_3}\left\{\frac{\partial J_3}{\partial\sigma}\right\} \tag{9}$$

where scalars $\partial F/\partial J_1$, $\partial F/\partial J_2$ and $\partial F/\partial J_3$ are the partial derivatives of yield function with respect to the three stress invariants and, therefore, their values depend on the feature of yield function. Rates $\{\partial J_1/\partial\sigma\}$, $\{\partial J_2/\partial\sigma\}$, and $\{\partial J_3/\partial\sigma\}$ are the gradient vectors of stress invariants. A strictly determinate form of the stress-strain relationship in nonlinear range can be obtained from Eq. 8 if explicit expression of the equivalent stress K in Eq. 1 is known.

2.3. Nonlinear Response of Concrete

Once the relation between the equivalent stress and the equivalent plastic strain, $\bar{\varepsilon}_p$, is defined, the strain hardening coefficient, H', along the ascending branch can be uniquely defined as

$$H'=\frac{\partial K}{\partial\bar{\varepsilon}_p} \tag{10}$$

In plasticity, the equivalent stress-strain relation has to be a single nonlinear curve. On the other hand, the experimental curves under biaxial stress are shown in Fig. 6 as plotted in Ref. 8. It can be observed that the curve at $\theta=60°$ gives much larger strain than that at $\theta=0°$ at the same stress level. This phenomenon is mainly caused by the effect of microcracking on nonlinear behavior of concrete, an effect which increases with increase in the ratio of biaxial stresses. This suggests that the approximation with a single curve could not simulate the exact

nonlinear response as demonstrated in Ref. 9. This problem could be overcome by introducing a model of an effective equivalent stress-strain relation that depends on the Lode angle as well as the equivalent plastic strain. This model can be taken into account in the incremental scheme so as to simulate the effect of microcracking as shown in Fig. 7. An assumed influence of the Lode angle on the $K-\bar{\varepsilon}_p$ relation is represented analytically first by defining the shape of the curves for $\theta=0°$ and 60°, and then specifying a function to interpolate between these curves as described in the following paragraph.

An exponential function was defined to modify the curves for $\theta=0°$ and 60° as

$$\begin{aligned} K_1&=a(1-e^{-c_1\bar{\varepsilon}_p})+b \qquad \text{for} \quad \theta=0° \\ K_2&=a(1-e^{-c_2\bar{\varepsilon}_p})+b \qquad \text{for} \quad \theta=60° \end{aligned} \tag{11}$$

where a, b, c_1 and c_2 are material constants and can be determined so as to coincide with the experimental stress-strain curves under uniaxial and biaxial compression using the boundary condition and initial yield strength, f_0, as

$$\begin{aligned} &a=(1/\sqrt{3}-\alpha)(f_c'-f_0), \quad b=f_0(1/\sqrt{3}-\alpha) \\ &c_1=H_{01}'/a, \quad c_2=H_{02}'/a \end{aligned} \tag{12}$$

The constants H_{01}' and H_{02}' are the effective strain hardening coefficients at $\theta=0°$ and 60° on the initial yield surface, respectively.

For a given state of stress in the region of $0°\leq\theta\leq60°$, a cosine interpolation function for the description of K in Eq. 1 is proposed in the form

$$K(\theta,\bar{\varepsilon}_p)=\frac{K_1+K_2}{2}+\frac{K_1-K_2}{2}\cos 3\theta \tag{13}$$

which satisfies continuity with respect to θ and $\bar{\varepsilon}_p$.

Note that Eq. 13, by its characteristic, is asymtotic to $K=f_c'(1/\sqrt{3}-\alpha)$ if $\bar{\varepsilon}_p\to\infty$.

Therefore, the term K at the maximum plastic strain involves a small error on the response, but this amount is negligible.

Now, by substituting Eq. 11 into Eq. 13 and differenciating it, the effective hardening coefficient H' for a given state of stress and strain can be derived as

$$H'=\frac{1}{2}[H_{01}'e^{-c_1\bar{\varepsilon}_p}+H_{02}'e^{-c_2\bar{\varepsilon}_p}+(H_{01}'e^{-c_1\bar{\varepsilon}_p}-H_{02}'e^{-c_2\bar{\varepsilon}_p})\cos 3\theta] \tag{14}$$

In addition, the three scalar values of the invariant derivatives defined in Eq. 9 can, now, be obtaind after some transformation as

$$\begin{aligned} \frac{\partial F}{\partial J_1}&=\alpha \\ \frac{\partial F}{\partial J_2}&=\frac{1}{2\sqrt{J_2}g(\theta)}\left[1-\frac{g'(\theta)}{g(\theta)}\cot 3\theta\right]+\frac{3}{4J_2}(K_1-K_2)\cos 3\theta \\ \frac{\partial F}{\partial J_3}&=\frac{\sqrt{3}}{2J_3}\left[\frac{g'(\theta)}{g(\theta)^2\sin 3\theta}+\frac{3}{4\sqrt{J_2}}(K_1-K_2)\right] \end{aligned} \tag{15}$$

where $g'(\theta)$ is partial derivative of $g(\theta)$ with respect to θ.

The value of the maximum equivalent plastic strain $\bar{\varepsilon}_p(\theta)$ for $0°<\theta<60°$ can be also interpolated by a similar function for K using the extreme values $(\bar{\varepsilon}_p^c, \xi\bar{\varepsilon}_p^c)$ at $\theta=0°$ and 60°. That is

$$\bar{\varepsilon}_p^c(\theta)=\frac{1}{2}[1+\xi+(1-\xi)\cos 3\theta]\bar{\varepsilon}_p^c \tag{16}$$

where the term ξ is the ratio of the equivalent plastic strain at $\theta=0°$ to that at 60° (see Fig. 6, 7).

It remains to define the rules for unloading. Unloading criterion is that if the equivalent plastic strain increment $d\bar{\varepsilon}_p$ is negative, unloading has occurred at the corresponding point. Once unloading has occurred, the equivalent stress, K_{rev}, and plastic strain, $\bar{\varepsilon}_p^{rev}$, have to be remembered and the elastic stress-strain relation is recovered for further loading untill the stress level again reaches K_{rev}. If K returns to K_{rev}, nonlinearity reverts back tofollowing the rules for monotonically increasing load as illustrated in Fig. 7. However, the value of θ is usually different from that of θ_{rev}. So the curve from the reloading point $(K_{rev}, \bar{\varepsilon}_p^{rev})$ should be changed with the change of the stress state between pre- and post-unloading.

Concerning a modeling of the descending (or softening) branch after the compressive strength, the same method proposed in Ref. 10, 11 was adopted by extended use for multi-axial state of stress.

The proposed model of the equivalent stress-strain relation can be made visible as shown in normalized stress versus strain for the concrete in Ref. 12 in Fig. 8.

2.4. Cracking

Cracking of concrete has the most important and significant effect on the nonlinear response of reinforced concrete structures as mentioned in the previous section. Methods of modeling of cracking has been getting firmly fixed by recent studies (6, 8, 9, 10, 11) even though several problems are still remained unsolved. Several assumptions were made in order to analyze the progressive cracking of concrete for any loading history and discussed below.

(1) A crack forms in a plane normal to the direction of the maximum principal stress when the stress state exceeds one of the brittle failure surfaces given by Eq. 3. All forces corresponding to the maximum principal stress is redistributed to the system.

(2) Once a crack has formed, the tangent modulus in the direction perpendicular to the crack plane is reduced to a negligibly small value to avoid numerical instability of the stiffness matrix of the system. The shear modulus in the crack plane is set to be a preselected constant such that $0. \leq \gamma_G \leq 1.0$ where γ_G is a shear retention factor due to aggregate interlock.

(3) As the load increases, further cracks can occur when the brittle failure conditions of Eq. 3 are exceeded. Three crack planes are possible at each stress evaluation point. In addition, crack closing is examined at every crack plane by means of strains.

3. Numerical Solution

Several procedures were successfully employed in the numerical solution so as to make the expected results refined.

(1) Steel is assumed to be an elastic-plastic strain hardening material related to the well-known Von Mises yield condition allowing elastic unloading.

(2) A method of discrete idealization of reinforced concrete structures was incorpolated in a suitable form for the computer program which utilizes 20-node brick element, 8-node membrane element, and 3-node axial element.

(3) A reduced numerical integration scheme with independent choice of integration points (2 or 3) in any direction in each element.

(4) The method of Euclidian displacement and force norm as a convergence criterion together with the modified Newton-Raphson procedure.

(5) Numerical refinements in determination of stress increments such as Nayak's over-shoot method to examine what kind of failure firstly occurs by new stress increment, and stress correction due to drift from the yield surface.

4. Numerical Examples

Three numerical examples were analyzed to investigate the feasibility of the nonlinear analysis developed. The first case was calculation of the two-dimensional response of the plain

concrete, to be compared with the data from Ref. 12. The second case involved the analysis of a small-scale axisymmetric PCRV test model with a solid end slab (Fig. 10). The third was the analysis of a three-dimensional PCRV test model with penetrations in the end slab (Fig. 10). The PCRV test models have been tested to investigate the shear failure of flat end slabs of PCRV under increasing internal pressure at the Structural Research Laboratory of the University of Illinois (13). Properties of materials used are listed in Table 1.

4.1. Biaxial Stress State

The analytical and experimental stress-strain relations under uniaxial and biaxial compression are compared in Fig. 9. It can be said that the failure and yield criteria proposed are acceptable for the approximation of nonlinear response of biaxial concrete.

4.2. Axisymmetric PCRV Test Model (Solid End Slab)

Fig. 11 illustrates the finite element mesh including the steel base plate in a 30-degree slice of axisymmetric PCRV test model designated PV28. Unbonded vertical steel tendons were simulated by external forces which were varied during the loading process to account for changes in stress. Computation time for this model with nine load increments and a maximun of four iteration cycles for each increment was about 280 sec on the CDC Cyber 175.

Pressure-Deflection Curves: Figure 12 shows the comparison of the measured and calculated deflections at the center of the end slab. The calculated initial tangent stiffness was slightly less than the measured one. The first cracking occurred in the radial direction of the end slab at 1.5 ksi (10.3 MPa) internal pressure. The calculated small decrease in the slope of pressure-deflection curve beyond 1.5 ksi was due to gradual development of "internal cracks". The observed failure pressure was 3.77 ksi (26.0 MPa), 7% more than the calculated value of 3.5 ksi (24.1 MPa).

Calculated Damage Pattern: Internal damage patterns of concrete at three pressure levels (2.5, 3.25 and 3.5 ksi) are shown in Fig 13. Damage patterns in this figure were modified by "smearing" the failure index information at each integration point over a tributary region half way to the next integration point. The calculated damage patterns provide a useful guide to interpreting the internal failure process of structure.

Deflected Shape: Calculated deflected shapes of PV28 are shown in Fig. 14 for three load levels of pressure. Solid lines in this figure indicate the original shapes and broken lines indicate the deflected shapes in exaggerated scale. Changes in the shape of PV28 with internal pressure can be clearly seen from this figure.

4.3. Three-Dimensional PCRV Test Model (End Slab with Penetrations)

Figure 15 shows a finite element mesh and the prestressing forces for the analytical model which represents a 30-degree section of a PCRV test model designated PV32 in Ref. 13. The load corresponding to the pressure on the cross section of the penetration applied to the finite element model as an equivalent line load around the circumference of the opening. Computation time for PV32 with ten load increments and a maximum of three iteration cycles at each load increment was approximately 400 sec.

Pressure-Deflection Curve: Figure 16 compares the experimental and calculated deflections at the center of end slab. Very good agreement between the experimental and calculated deflections was obtained throughout the entire loading ranges. The calculated maximum pressure was 2.95 ksi (20.3 MPa), while the experimental failure pressure was 3.08 ksi (21.3 MPa) corresponding to a 4.0% difference in pressure between the physical and the analytical models at failure.

Calculated Damage Pattern: Calculated damage patterns of concrete at two pressure levels (2.5 and 2.95 ksi) in two different vertical cross sections are shown in Fig. 17, 18. Cracking

initiated radially at the upper center of end slab at 1.5 ksi (10.3 MPa) and progressed along the upper surface with the increase of pressure. Yielding in compression firstly occurred at the midheight portion of the penetration at 1.5 ksi and developed vertically downward. From the figures of the final damage patterns, the concrete around the penetration was severely damaged in both sections. Crushing of concrete, where the equivalent strain entered in the range of "descending branch", was caused in some regions of section $A-A$. It can be referred from the calculation that the strength of the test vessel would be limited by cracking and crushing failure of the concrete around the penetration.

It is of interest to compare the damage patterns near maximum pressure for PV28 and PV32. While the distribution of damage over the section of PV28 was general and the dome thrust line could be seen, the damage in PV32 was concentrated at or near the section of the penetration.

Deflected Shape: The deflected shape of PV32 at representatives of pressure are shown in three-dimensions in Fig. 19. Distorsions which occur before failure are emphasized in the figure suggesting that the nonlinear response of this model was influenced strongly by the failure of concrete around the penetration.

5. Conclusion

This report develops a three-dimensional finite element model for simulating the nonlinear response of reinforced concrete structures such as PCRV's under monotonically increasing internal pressure.

The analytical model has been tested using experimental results from (1) plain concrete tested under biaxial compressive stresses, (2) test of a cylindrical prestressed concrete pressure vessel model with a solid end slab, and (3) test of a similar vessel with an end slab containing penetrations.

Comparisons between the experimental and calculated results were satisfactory in each case in spite of the relatively coarse mesh. Though the shear retention factor in a cracked plane was assumed to be zero for all cases, the calculated responses of the test vessels indicated good agreements with the experimental results.

6. Acknowledgements

The work leading to this report was carried out in the Structural Research of the Department of Civil Engineering, University of Illinois, Urbana.

The writer acknowledges his gratitude for advice from Professors M. A. Sozen, W. C. Schnobrich, and D. A. Pecknold.

7. References

1) Richart, F. E., et al.: A study of the Failure of Concrete under Combined Compressive Stresses, Engineering Experiment Station, University of Illinois, Bulletin No. 185, (1928).
2) Launacy, P., et al.: Strain and Ultimate Strength of Concrete under Triaxial Stress, ACI Special Publ. SP-34, (1972).
3) Kobayashi, S., et al.: Failure Criterion of Concrete Subjected to Multi-Axial Compression, Journal of Materials, Vol. 16, No. 170, Japan, (Nov. 1967).
4) Linse, D.: Losung Versuchstechnisher Fragen bei der Ermittlung des Festigkeits-und Verformungsverhaltens von Beton unter Dreiachsinger Belastung, Deutscher Ausschuss Fur Stahlbeton, HEFT 292, Berlin, (1978).
5) Cedolin, L., et al.: Triaxial Stress-Strain Relationship for Concrete, Jour. of ASCE, EM3, (Jun. 1977).
6) Argyris, J. H., et al.: Recent Developments in the Finite Element Analysis of Prestressed Concrete Reactor Vessels, Nucl. Eng. (Des. 28, 1974).
7) Nagamatsu, S., et al.: Study on Failure Criterion of Concrete under Combined Stresses (Part 1-3), Trans. of AIJ, No. 246, 247, 254, (Aug., Sept. 1976 and Apr. 1977).
8) Chen, A. C. T., et al.: Constitutive Relations for Concrete, ASCE, EM4, (Aug. 1975).
9) Noguchi, H.: Finite Element Nonlinear Analysis of Reinforced Concrete (Part 1), Trans. of AIJ, No. 252,

(Feb. 1977).
10) Imoto, K.: Elastic-Plastic Analysis of Reinforced Concrete Members by the Finite Element Method, Proc. Annual Con., AIJ, (Oct. 1973).
11) Darwin, D., et al.: Analysis of R. C. Shear Panels under Cyclic Loading, ASCE, Vol. 102, No. ST2, (Feb. 1976).
12) Kupfer, H., et al.: Behavior of Concrete under Biaxial Stresses, J. of ACI, Proc. 66 (8), (Aug. 1969).
13) Reins, J. D., et al.: Shear Strength of End Slabs of Prestressed Concrete Nuclear Reactor Vessels, Struc. Research Series No. 429, Univ. of Illinois, (Jul. 1976).

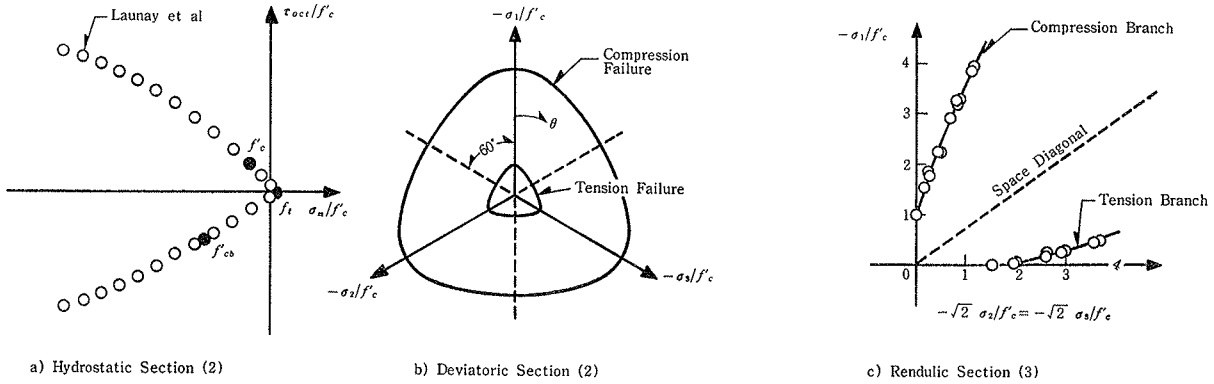

a) Hydrostatic Section (2) b) Deviatoric Section (2) c) Rendulic Section (3)

Fig. 1 Experimental failure surface of concrete under multiaxial stress state

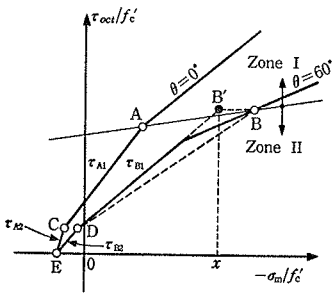

coordinates

	σ_1/f_c'	σ_2/f_c'	σ_3/f_c'	$-\sigma_m/f_c'$	τ_{oct}/f_c'
A	0	0	−1.0	$\frac{1}{3}$	$\frac{\sqrt{2}}{3}$
B	0	$-\eta_b$	$-\eta_b$	$\frac{2}{3}\eta_b$	$\frac{\sqrt{2}}{3}\eta_b$
C	β_t	β_t	0	$-\frac{2}{3}\beta_t$	$\frac{\sqrt{2}}{3}\beta_t$
D	β_t	0	0	$-\frac{1}{3}\beta_t$	$\frac{\sqrt{2}}{3}\beta_t$
E	β_t	β_t	β_t	$-\beta_t$	0

f_c' : uniaxial compressive strength
f_t : uniaxial tensile strength
η_b : biaxial compressive stength ratio
$\beta_t = f_t/f_c'$ $(\eta_b = 1.0 \sim 2.0)$

Fig. 2 Experimentally confined points on the failure surface

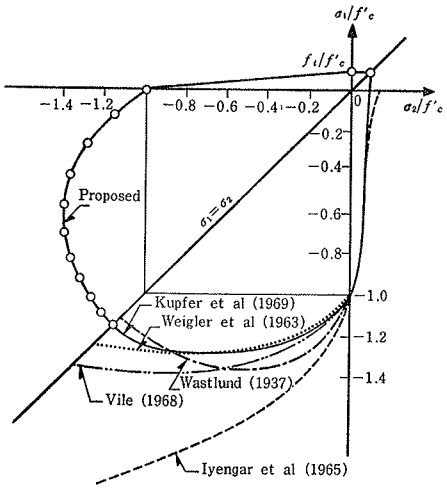

Fig. 3 Comparison of proposed and experimental biaxial failure envelopes (4)

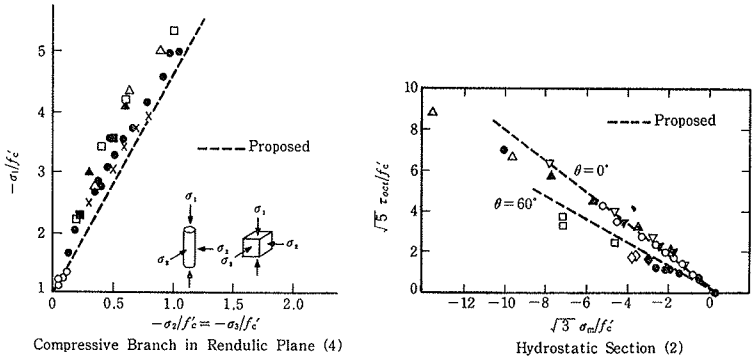

Compressive Branch in Rendulic Plane (4) Hydrostatic Section (2)

Fig. 4 Comparison of fits with experimental data along meridians

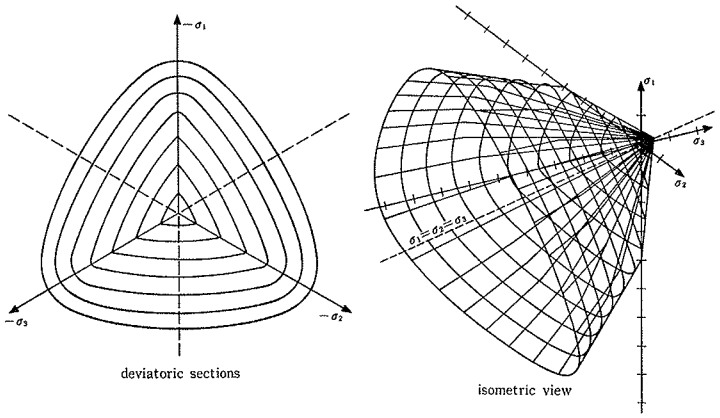

Fig. 5 Failure surface of proposed model

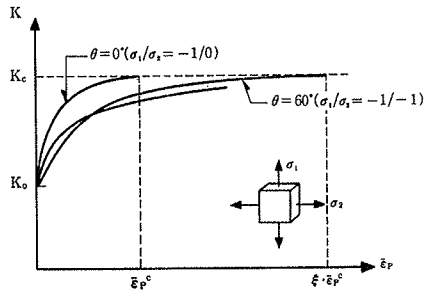

Fig. 6 Experimental equivalent stress-strain relations (8)

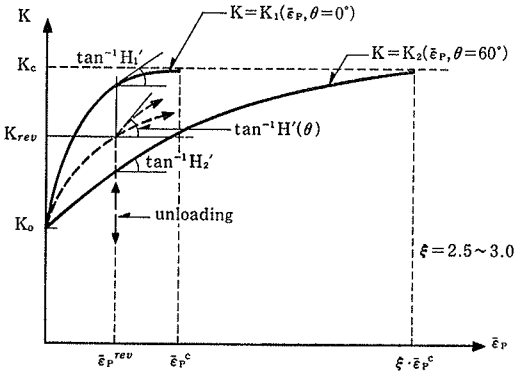

Fig. 7 A model of equivalent stress-strain relations

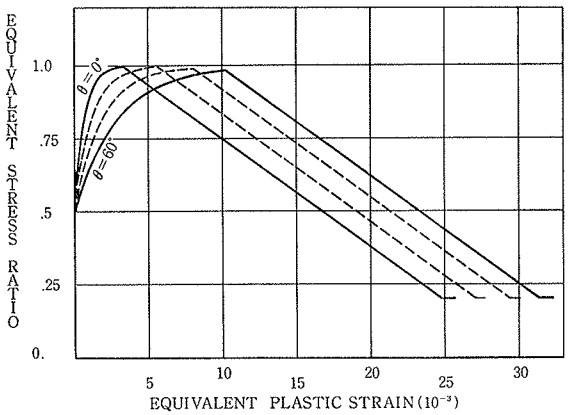

Fig. 8 Analytical model of equivalent stress-strain curves ($\xi=3.0$)

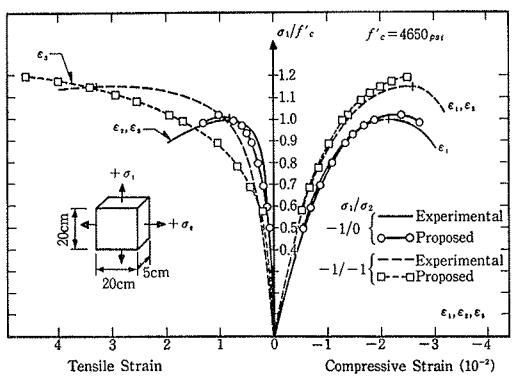

Fig. 9 Stress-strain relations under biaxial compression (12)

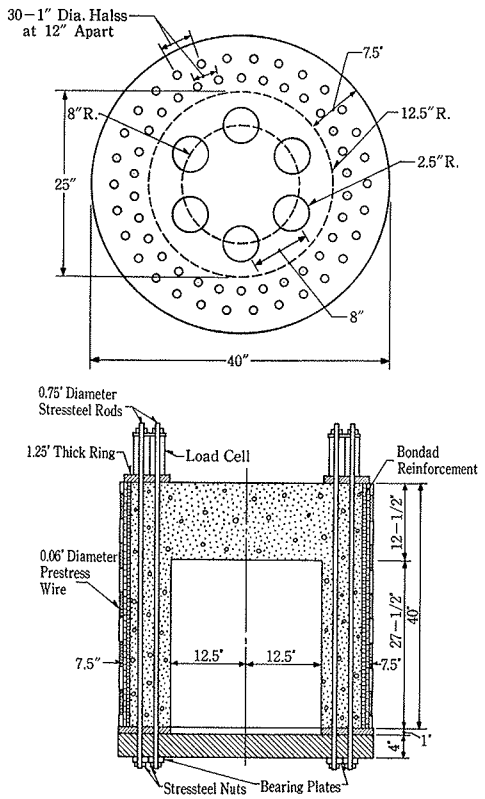

Fig. 10 PCRV test models (13)

	Concrete Properties in psi (MPa)		
	Two-Dimensionl Plain Concrete (2)	Axisymmetric PV28(13)	Three-Dimensional PV32(13)
E_1	4.28×10^6(227,500)	3.9×10^6(26,900)	3.8×10^6(26,900)
E_2	-0.85×10^6(−5,900)	-0.85×10^6(−5,900)	-0.85×10^6(−5,700)
f_c'	4,650(32.1)	6,420(44.3)	5,720(39.4)
f_t	430(2.96)	440(3.0)	450(3.1)
ε_c	0.00216	0.0028	0.00263
ε_x	0.00137	0.0018	0.00178
Constants	$f_0=0.5f_c'$, $\sigma_x=0.9f_c'$, $\eta_b=1.16$, $\beta=0.75$, $\xi=3.0$, $\nu=0.15$, $\gamma_G=0.0$ (shear factor)		
	Steel Properties for PV28 and PV32 in psi (MPa)		
	Liner and Base Plate	Vertical Tendon	Circumterential Wire
E_1	30×10^6(210,000)	29×10^6(200,000)	30×10^6(210,000)
E_{st}	$0.05E_1$	$0.04E_1$	$0.04E_1$
σ_y	40,000(275)	140,000(961)	280,000(1,940)
ν	0.3	0.3	0.3
ε initial	——	0.0035	0.004

Table 1. Properties of materials assumed for analysis

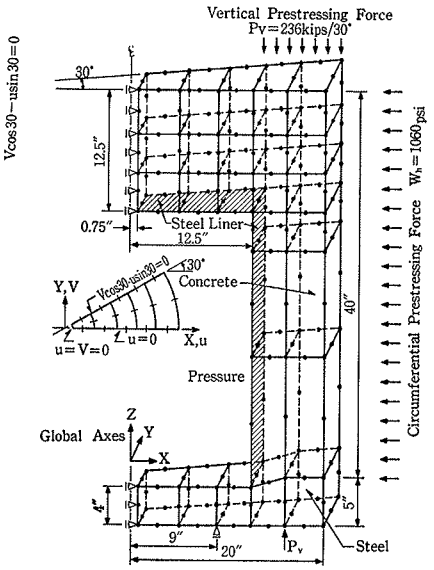

Fig. 11 Finite element idealization of PV 28

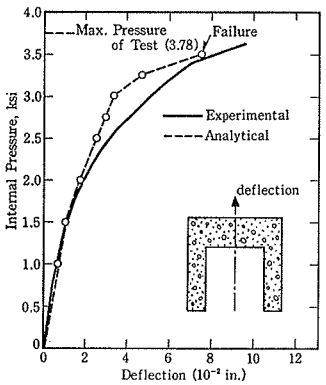

Fig. 12 Measured and calculated deflections at the center of the end slab for PV28

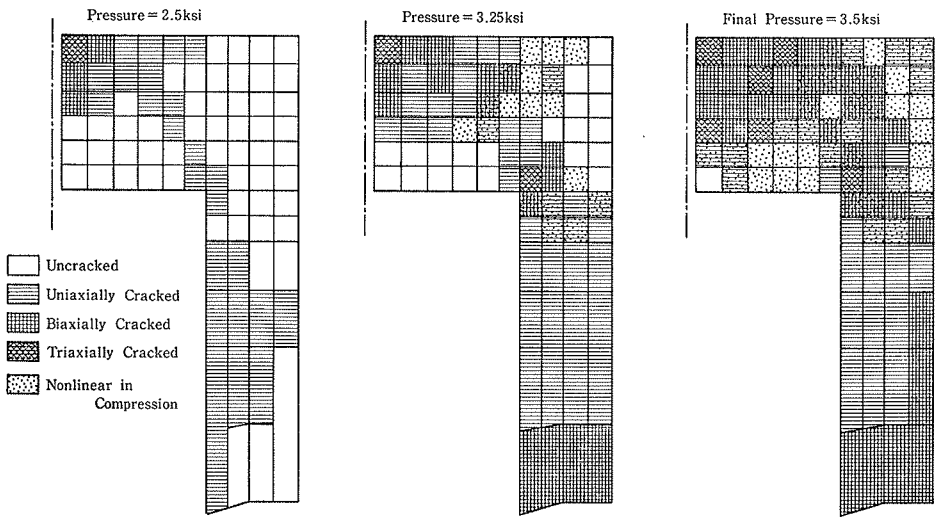

Fig. 13 Calculated damage patterns of PV28 at three pressure levels (2.5, 3.25 and 3.5 ksi)

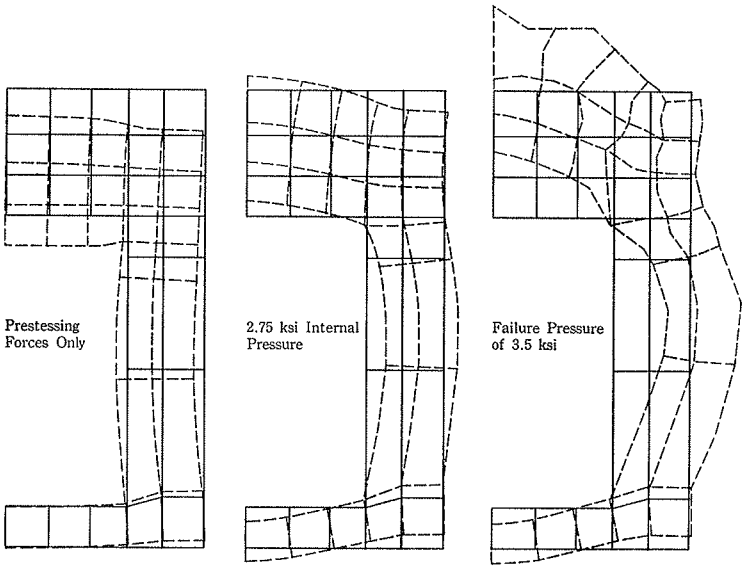

Fig. 14 Deflected shapes of PV28

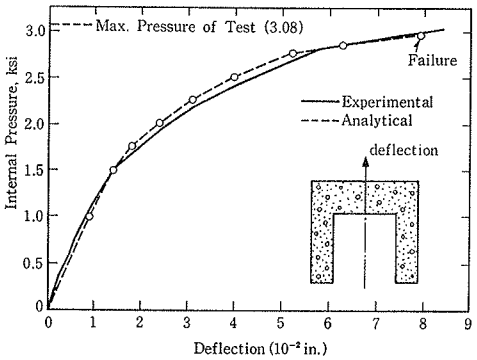

Fig. 16 Measured and calculated deflections at the center of the end slab for PV32

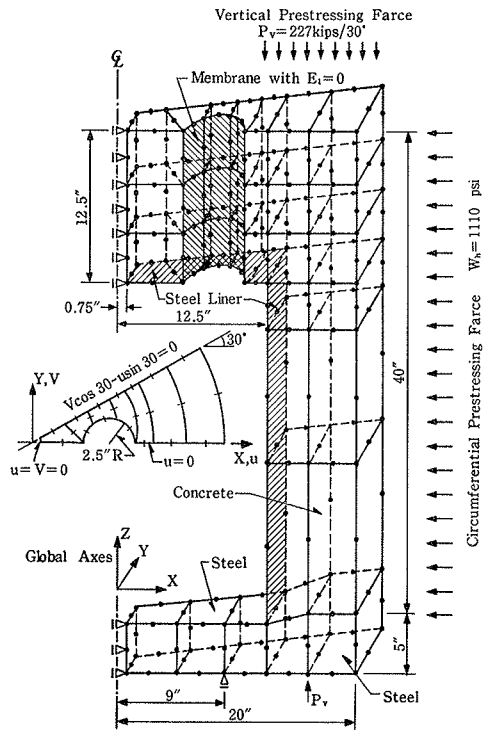

Fig. 15 Finite element idealization of PV32

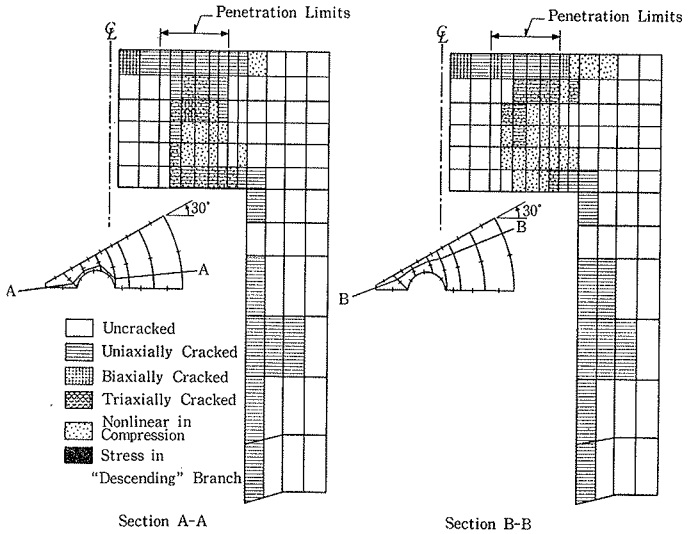

Fig. 17 Damage patterns of PV32 at 2.5 ksi internal pressure

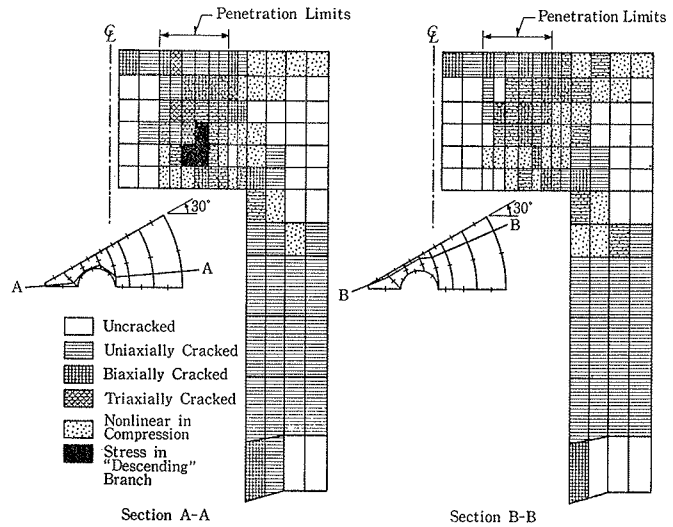

Fig. 18 Final damage patterns of PV32 at 2.95 internal pressure

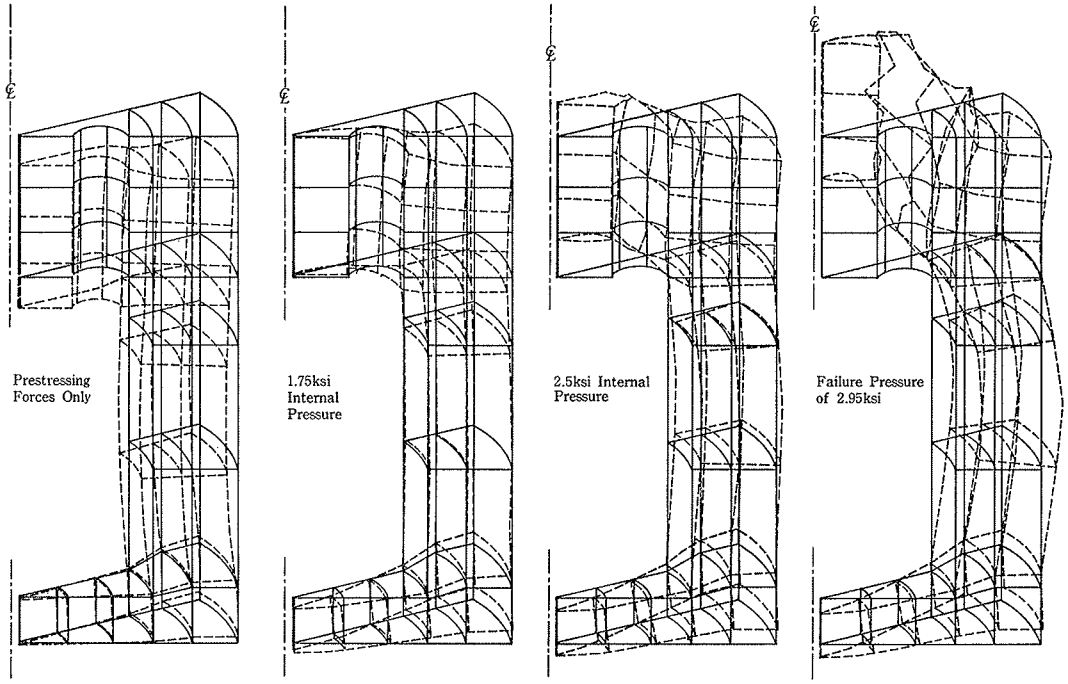

Fig. 19 Deflected shapes of PV32